ELSEVIER

Surface Science 479 (2001) 11–25

SURFACE SCIENCE

www.elsevier.nl/locate/susc

Adsorption of CO on $Cr_2O_3(0\,0\,0\,1)$

M. Pykavy [a], V. Staemmler [a,*], O. Seiferth [b], H.-J. Freund [b]

[a] *Lehrstuhl für Theoretische Chemie, Ruhr-Universität Bochum, Universitäts-strasse 150, D-44780 Bochum, Germany*
[b] *Fritz-Haber-Institut der Max-Planck-Gesellschaft, Faradayweg 4-6, D-14195 Berlin-Dahlem, Germany*

Received 31 May 2000; accepted for publication 15 February 2001

Abstract

The adsorption of CO molecules on the Cr-terminated (0 0 0 1) surface plane of Cr_2O_3 is studied theoretically by means of quantum chemical cluster calculations and experimentally by thermal desorption spectroscopy and infrared reflection absorption spectroscopy. The combination of these approaches yields a detailed picture of the CO/$Cr_2O_3(0\,0\,0\,1)$ adsorption. In the low coverage limit, CO is strongly bound (chemisorbed) and occupies a O_3-hollow position, i.e. it is adsorbed above a threefold hollow site in the first full oxygen layer, with the CO axis oriented along a line connecting two Cr ions at the surface and tilted strongly against the surface normal. CO molecules in this position desorb at 175 K, which corresponds to an adsorption energy of 45 kJ/mol, and exhibit a blue shift of the CO stretching frequency of about 35 cm^{-1} with respect to CO in the gas phase (from 2143 to 2178 cm^{-1}). At higher coverages, a second desorption peak at 105 K is found which is accompanied by a small red shift of -10 cm^{-1} of the CO stretching frequency. This adsorption state corresponds to a physisorption of CO with an adsorption energy of 28 kJ/mol and is tentatively assigned to CO molecules adsorbed parallel to the surface above one O^{2-} anion in the oxygen layer.

Keywords: Chromium; Carbon monoxide; Clusters; Thermal desorption spectroscopy; Infrared absorption spectroscopy; Ab initio quantum chemical methods and calculations

1. Introduction

The adsorption of CO on α-Cr_2O_3 has been the subject of several experimental studies in the past 15 years. The techniques most frequently applied were low-energy electron diffraction (LEED) [1,2], angular resolved ultraviolet photoelectron spectroscopy (ARUPS) [1,2], and infrared spectroscopy [3–11]. However, the results of these studies are hardly comparable since the LEED and ARUPS experiments were performed at low temperatures on carefully prepared and well ordered $Cr_2O_3(0\,0\,0\,1)$/Cr(1 1 0) films [1,2], while in most of the IR studies polycrystalline powder samples, i.e. α-Cr_2O_3 microcrystals, were employed which show several different crystal faces.

Therefore, several questions concerning the geometrical structure and the energetics of the system CO/$Cr_2O_3(0\,0\,0\,1)$ remain open currently:

(a) ARUPS and near edge X-ray absorption fine structure (NEXAFS) data [1,2] led to the conclusion that a single CO molecule adsorbs parallel or strongly tilted on the $Cr_2O_3(0\,0\,0\,1)$ surface.

* Corresponding author. Tel.: +49-234-3226752; fax: +49-234-3214045.
E-mail address: staemm@mokat50.theochem.ruhr-uni-bochum.de (V. Staemmler).

0039-6028/01/$ - see front matter
PII: S0039-6028(01)00975-X

However, this orientation was questioned, mainly because the observed blue shift of the CO stretching frequency seemed to be indicative for a perpendicular adsorption of CO on top of one Cr^{3+} surface ion [11].

(b) A precise value for the adsorption energy of CO on $Cr_2O_3(0\,0\,0\,1)$ is not known. And, despite of several IR studies, the CO stretching frequency for this system is not known as well since none of the IR bands observed in powder samples seems to be attributable to CO adsorbed on the $(0\,0\,0\,1)$ face of Cr_2O_3 [11].

(c) In the LEED experiments of Xu et al. [1] an unusual $(\sqrt{3}\times\sqrt{3})R30°$ structure of CO/$Cr_2O_3(0\,0\,0\,1)$ at monolayer coverage was detected. So far it is not clear why such a structure is formed: probably, it reflects the most favorable adsorption position of a single CO molecule on $Cr_2O_3(0\,0\,0\,1)$, but it is also possible that lateral interactions between adsorbed CO molecules play a role. Another possibility is an adsorbate-induced reconstruction of the $Cr_2O_3(0\,0\,0\,1)$ surface itself.

In the present paper we attempt to answer some of these questions in a combined theoretical and experimental study. In a series of ab initio embedded cluster calculations we calculate the adsorption geometry and energy and the frequency of the CO stretching vibration of a single CO molecule adsorbed on the $Cr_2O_3(0\,0\,0\,1)$ surface. Parallel to these calculations, thermal desorption spectroscopy (TDS) and infrared reflection absorption spectroscopy (IRAS) experiments are performed to compare the adsorption energy and the CO stretching frequency with the results of the calculations.

The potential energy surface calculated in the present study for the system CO/$Cr_2O_3(0\,0\,0\,1)$ will be used in a forthcoming study [12] for Monte Carlo simulations of the geometrical structure of a CO monolayer on $Cr_2O_3(0\,0\,0\,1)$.

2. Method of calculation

All theoretical results presented in this paper were obtained by means of quantum chemical embedded cluster calculations. The electronic structure of the system CO/$Cr_2O_3(0\,0\,0\,1)$ is described by wave function based ab initio methods, in which the $Cr_2O_3(0\,0\,0\,1)$ surface is represented by a finite cluster embedded in an extended array of point charges (Madelung field).

2.1. Geometrical structure of the $Cr_2O_3(0\,0\,0\,1)$ surface

α-Cr_2O_3 has corundum-type structure [13] with alternating hexagonal closed packed (hcp) oxygen layers and slightly buckled Cr double layers. The stoichiometry of the crystal is achieved by the fact that only two out of three octahedral positions in the Cr double layer are occupied by Cr ions and one position remains empty. This leads to slight lateral distortions in the planar hcp oxygen layers.

The Cr terminated $(0\,0\,0\,1)$ surface plane of Cr_2O_3 is a polar surface and therefore thermodynamically unstable [14–16]. It is now well established, both theoretically and experimentally, that this surface is stabilized by the removal of 50% of the Cr ions in the topmost Cr layer. By such a reduction of the surface charge density the divergence of the Madelung energy is avoided [14,15]. In addition to this reconstruction, large geometrical and electronic relaxations have been found at the surface: the charges of the chromium and oxygen atoms in the first two layers are considerably reduced, from $+3.0$ and -2.0 in the bulk to about $+2.1$ and -1.7 at the surface [17]. More importantly, the first four interlayer distances deviate strongly from the respective bulk values. Table 1 contains the results of several recent experimental and theoretical studies. Apparently, there is good qualitative agreement between the data obtained by the various theoretical approaches and the LEED experiments. However, the exact amount of the relaxation of the topmost Cr–O interlayer distance is still uncertain. The most recent periodic SCF calculations [21] agree very nicely with the improved $I(V)$ analysis of the LEED data [23] as far as the distances b, c, d are concerned, but disagree considerably in the first Cr–O interlayer distance a.

Unfortunately, the adsorption energy of CO on the $Cr_2O_3(0\,0\,0\,1)$ surface depends rather sensitively on the first Cr–O interlayer distance a, as we will see later. In order to eliminate this source of

Table 1
Relaxation of the first four interlayer distances at the $Cr_2O_3(0001)$ surface (in % relative to the bulk values)[a,b]

Method	*a*	*b*	*c*	*d*	Reference
MD simulations	−58	0	−36	+17	[18]
Empirical AIM[c] potential	−40	+6	−30	+11	[19]
ab initio SCF (UHF)	−50	+3.3	–[d]	–[d]	[20]
ab initio SCF (ROHF)	−45	−4	−24	+9	[21]
FP-LAPW	−59	+1	−38	+10[e]	[22]
LEED analysis	-38 ± 4	-21 ± 6	-25 ± 16	$+11 \pm 9$	[18]
Improved LEED analysis	−60	−3	−21	+6	[23]

[a] *a*, *b*, *c*, *d* denote the first four interlayer distances.
[b] *a*, *b*, and *d* correspond to the Cr–O interlayer distances which are 0.94 Å, while *c* is the distance within the Cr double layer and amounts to 0.38 Å [13].
[c] AIM means 'aspherical ion model'.
[d] Not varied.
[e] The relaxation of the fifth interlayer distance was also included and found to be −4%.

uncertainty, we have tried to obtain an alternative estimate for *a*, more consistent with the present cluster calculations and independent from the previous theoretical results, all of which are based on periodic models. To this purpose we have optimized the Cr–O interlayer distance of a CrO_3^{3-} cluster embedded in a large point charge (PC) field (for details see Section 2.2). All but the topmost Cr–O interlayer distances in the embedding PC field were fixed at the improved LEED values (see Table 1); the topmost interlayer distance was held at an inward relaxation of either 60% or 40% as compared to the bulk Cr–O interlayer distance. Fig. 1 shows that in both cases the energy minimum is found for a Cr–O distance in the CrO_3^{3-} cluster which corresponds to a relaxation of about 35%. This means that a consistent description is obtained for a relaxation of about 40%, both in the cluster and in the embedding PC field.

This result is in good agreement with the periodic SCF calculations as well as with the older LEED analysis (compare Table 1). The reason that the MD simulations [18] yield a larger relaxation of 58% can be attributed to the fact that the full ionic charges of +3 and −2 were used for the surface as for the bulk, therefore the interlayer attraction at the surface is too strong. Although the improved LEED analysis [23] favors a strong relaxation of 60% as well as we think that a value of about 40% is more realistic.

It should be noted that Gloege et al. [24] performed an X-ray analysis of the $Cr_2O_3(0001)$ surface recently and found evidence for Cr interstitials and a very small inward relaxation of only 6% at the surface. This observation is in disagreement with the present cluster calculations as well as with all results collected in Table 1.

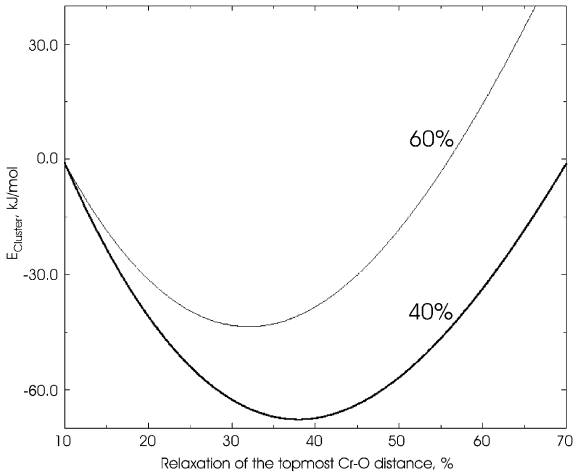

Fig. 1. Energy of the embedded CrO_3^{3-} cluster as a function of the relaxation of the Cr–O distance in the cluster. The relaxation of the topmost interlayer distance in the embedding PC field was fixed at 40% or 60%.

2.2. Embedded cluster models

In order to describe the adsorption of CO at different adsorption sites above the $Cr_2O_3(0001)$ surface with comparable accuracy, it is necessary to use cluster models which contain several Cr^{3+}

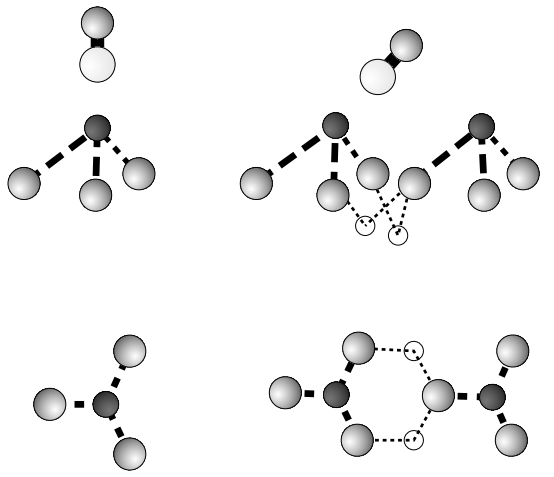

Fig. 2. Side view (with adsorbed CO) and top view (without CO) of the CrO_3^{3-} and Cr_4O_6 clusters used to describe the $Cr_2O_3(0001)$ surface. Full spheres: surface Cr^{3+} ions, hatched spheres: O^{2-} anions, empty spheres: Cr^{3+} ions in the third layer. The latter two Cr^{3+} ions are replaced with point charges in the $Cr_2O_6^{6-}$ cluster.

ions at the surface and the adjacent O^{2-} anions in the second layer explicitly and which are embedded in a carefully chosen PC field. The clusters employed in the present study are shown in Fig. 2.

The smallest possible cluster that can be used to treat the adsorption of CO on the $Cr_2O_3(0001)$ surface has the composition CrO_3^{3-} and consists of one Cr^{3+} ion in the topmost layer and the three neighboring O^{2-} anions in the second layer. Such a small cluster is only appropriate for the atop adsorption of CO on one Cr^{3+} ion at the surface. For adsorption geometries in which CO is adsorbed strongly tilted or parallel to the surface along the line connecting two Cr^{3+} surface ions it is necessary to extend the size of the cluster in such a way that it contains at least two Cr^{3+} ions in the topmost layer and all their O^{2-} neighbors in the second layer. This $Cr_2O_6^{6-}$ cluster has been used in most of our calculations. The stoichiometric neutral Cr_4O_6 cluster containing two more Cr^{3+} ions in the third layer may provide a slightly better description of the electrostatic potential above the surface in the region between the two Cr^{3+} surface ions, however, the adsorption geometries and energies calculated for CO on the embedded $Cr_2O_6^{6-}$ and Cr_4O_6 clusters differ only insignificantly.

The long-range electrostatic effects above the $Cr_2O_3(0001)$ surface are accounted for by embedding the clusters in an extended PC field. As in our previous work [25] we used the technique of fractional charges to speed up the convergence of the Madelung energy as a function of the size of the PC field. This technique has first been proposed by Evjen [26] and later extended by Stolarczyk and Piela [27] and Piela et al. [28] who added artificial fractional charges at the borders of the unit cell in order to eliminate its lowest multipole moments. When the size of the PC field is extended by the addition of more and more unit cells the fractional charges at all inner boundaries cancel or add up to the true ionic charges; partial charges survive only at the outermost borders. The virtue of this construction is that low multipole moments are zero or small irrespective of the size of the PC field and that the Madelung energy as well as the electrostatic potential above the surface converge quite rapidly.

In the case of Cr_2O_3, a unit cell consisting of 46 point charges (as compared to the minimum number of 30 ions in the hexagonal unit cell [13]) could be constructed, the multipole moments of which are rather small, though not entirely zero. Fortunately, the adsorption of a neutral molecule, in particular that of CO which has only a small dipole moment, is quite insensitive to long-range electrostatic effects. This is completely different for the adsorption of charged species, such as for instance O^- or O_2^- [29]. For generating an electrostatic field above the $Cr_2O_3(0001)$ surface that has the same accuracy for all possible adsorption positions of CO, it was compulsory to use a rather extended PC array, which contained the central unit cells at the adsorption site and four neighboring cells in each lateral direction as well as two cells perpendicular to the surface. The whole PC field consisted of 5826 point charges.

In order to avoid huge dipole moments normal to the surface plane, all PC fields were constructed in such a way that the same reconstruction and relaxation which had to be made in the topmost layers (containing the cluster) were also made in the bottom layers. In particular, both the topmost and the bottom Cr layers contained only half the number of positive point charges as the inner Cr layers.

It has been observed several times that the electrons of the O^{2-} anions, which are included explicitly in the cluster, will float towards the cations in the embedding PC field if this contains unscreened positive charges. This effect is particularly strong when extended basis sets are used and leads to artificially large basis set superposition errors (BSSE). In order to avoid this effect we have added basis-free effective core potentials (ECPs) to all positive point charges immediately adjacent to one of the O^{2-} anions in the cluster. The Al-type ECPs generated by Bergner et al. [30] were used throughout.

The present calculations were performed for two different relaxations of the topmost Cr–O interlayer distance: 60% as in the improved LEED analysis [23] and 40% as given by most of the theoretical studies. In both cases, these relaxations were applied to the cluster itself and to the embedding PC field, both for the top and bottom layers. The next three interlayer distances *b*, *c*, and *d* were fixed at the values given by the improved LEED analysis [23] which are close to the best results from periodic Hartree–Fock calculations [21]. Furthermore, reduced ionicities of +2.0 (instead of +3) and −1.667 (instead of −2) in the first two layers were used for generating the PC field, since both cluster calculations [17] and periodic Hartree–Fock calculations [21] have shown that the partial charges of the Cr and O ions at the surface are considerably lower than in the bulk.

In a series of test calculations, the effect of adsorbate-induced relaxations of the topmost Cr–O interlayer distance has been checked. It was found that this effect is of minor importance, changing the adsorption energy by only 3–5 kJ/mol. Therefore, we decided not to vary the geometry of the $Cr_2O_3(0001)$ substrate during adsorption of CO. Similarly, the C–O bond distance was fixed at 2.132 a.u. in all calculations, except for those determining the CO stretching frequency.

2.3. Quantum-chemical methods

All calculations were performed by means of the Bochum suite of open-shell ab initio programs [31–34]. In most cases the SCF approach in the form of restricted open-shell Hartree–Fock (ROHF) [31] was used. Dynamic correlation effects have to be included if one is aiming at reliable adsorption energies and vibration frequencies. In the present study correlation effects were taken care of by the multiconfiguration coupled electron pair approach (MCCEPA) which yields a good approximation to a full multireference coupled cluster treatment [34].

Cr_2O_3 is supposed to be strongly ionic containing Cr ions in the oxidation state +3 and O^{2-} anions. Cluster calculations [17] as well as periodic SCF calculations [21] have shown that the ionicities of the Cr and O ions in bulk Cr_2O_3 are indeed close to +3 and −2, respectively. The isolated Cr^{3+} cation has the electronic configuration $[Ar]3d^3$ with a ^4F ground state. In the (slightly distorted) octahedral ligand field in bulk Cr_2O_3, the sevenfold spatially degenerate ^4F ground state of Cr^{3+} is split into a (spatially non-degenerate) $^4A_{2g}$ ground state with the configuration t_{2g}^3 and two low-lying excited states of $^4T_{2g}$ and $^4T_{1g}$ symmetry with excitation energies of about 1.7 and 2.7 eV, respectively [17]. At the $Cr_2O_3(0001)$ surface, the ligand field strength is considerably lowered and the local symmetry at the Cr^{3+} ions is reduced, therefore the excited $^4T_{2g}$ and $^4T_{1g}$ states are lowered in energy and their degeneracy is partially removed. However, the electronic ground state of a surface Cr^{3+} ion remains a spatially non-degenerate quartet state with three singly occupied 3d orbitals, but because of the larger covalency of the Cr–O bond at the $Cr_2O_3(0001)$ surface there is some charge transfer from the oxygen layer to the surface Cr ion such that the partial charge at Cr is reduced to 2.1 [17].

Thus, the Cr^{3+} ions both at the $Cr_2O_3(0001)$ surface and in bulk Cr_2O_3 have quartet ground states with three singly occupied 3d orbitals. Such states can be well described by a single-reference ROHF wave function. The Cr_nO_m clusters which we use to describe the $Cr_2O_3(0001)$ surface contain several of these Cr^{3+} ions. In all subsequent calculations, the singly occupied 3d orbitals at all Cr^{3+} ions are coupled to a high-spin state (ferromagnetic state) which can be described by a single-reference ROHF wave function as well. The experimentally observed antiferromagnetic coupling between adjacent Cr ions (superexchange

coupling through the oxygen bridges) has been neglected in the present study since it is rather small (with an exchange integral of about -85 cm^{-1} [35]) and has no influence on the interaction between the $Cr_2O_3(0001)$ surface and a closed-shell molecule like CO.

The O^{2-} anions of the cluster have closed-shell ^1S ground states with fully occupied K and L shells ($1s^2 2s^2 2p^6$). The CO molecule is of course a closed-shell molecule as well. That means that the whole system $CO/Cr_2O_3(0001)$ is fairly well described by a ROHF wave function, and so are the fragments CO and the Cr_2O_3 cluster.

The basis set used in most of the following calculations has essentially triple zeta (TZ) quality for the cluster and TZ2P quality (TZ augmented by two sets of polarization functions) for the approaching CO. The details are given in Table 2. The reason for using basis sets of different quality for adsorbate and substrate is that the bonding between CO and the surface has predominantly electrostatic character, i.e. it is caused by the interaction between the multipole moments of CO and the electrostatic field above the surface. The addition of polarization functions at the Cr^{3+} ions or the O^{2-} anions in the cluster does not markedly change the electrostatic field above the surface. Likewise, it is sufficient to describe the Cr^{3+} ions in the third layer at a lower level of accuracy. On the other hand, the calculated multipole moments of CO depend strongly on the basis set employed. The SCF results for the dipole and quadrupole moments of CO, calculated with the standard TZ2P basis as given in Table 2, are 0.101 (orientation C^+O^-) and 1.546 a.u., respectively. They are rather close to the experimental values of -0.044 and 1.44 a.u. [39], but with the wrong sign of the dipole moment. A further increase of the CO basis beyond TZ2P quality does not improve these properties substantially, while smaller basis sets yield much worse results. The MCCEPA values for the respective properties are -0.013 and 1.463 a.u., i.e. the quadrupole moment is rather good and the wrong sign of the CO dipole moment obtained in the SCF approximation is corrected.

Since the bonding between CO and Cr_2O_3-(0001) is rather weak, all calculated interaction energies have to be corrected for the BSSE. This was done in the present study by means of the full Boys–Bernardi [40] counterpoise method. In some cases we had to allow for fragment relaxations; the counterpoise corrected binding energy of the supermolecule in its geometry relative to the relaxed (equilibrium) geometries of the fragments is given by

$$\begin{aligned} E_{\text{bind}} = {} & E_{\text{AB}}(R; r_{\text{A}}, r_{\text{B}}; \text{AB}) \\ & - E_{\text{A}}(r_{\text{A}}; \text{AB}) + [E_{\text{A}}(r_{\text{A}}; \text{A}) - E_{\text{A}}(r_{\text{A}}^{\text{e}}; \text{A})] \\ & - E_{\text{B}}(r_{\text{B}}; \text{AB}) + [E_{\text{B}}(r_{\text{B}}; \text{B}) - E_{\text{B}}(r_{\text{B}}^{\text{e}}; \text{B})] \end{aligned}$$

where r_{A}^{e} and r_{A} denote the equilibrium and the distorted geometries of the fragment A, similar for fragment B, and the basis sets used for the individual calculations are given as the last entries in the parentheses. It is sufficient to calculate the distortion energies of the two fragments only in the respective fragment basis sets. A similar formula has been given recently by Xantheas [41].

2.4. Calculated adsorption geometry and energy

We have first performed a series of introductory calculations for CO above a pure PC charge field representing the $Cr_2O_3(0001)$ surface. It became quickly obvious that the interaction between CO and the surface is only attractive if CO is adsorbed

Table 2
Standard basis set used for the $CO/Cr_2O_3(0001)$ calculations

Atom	Standard contraction	Additional functions	Reference
Cr surface	14s9p5d → 9s6p4d	s(0.038)	[36]
Cr bulk	5s4p5d → 3s2p3d[a]		[37]
O cluster	9s5p → 6s3p		[38]
C CO	9s5p → 6s3p	d(1.0, 0.3)	[38]
O CO	9s5p → 6s3p	d(2.0, 0.5)	[38]

[a] This basis is used in conjunction with the small core pseudopotentials for the [Ne] core of Cr^{3+} [37].

along a line connecting two surface Cr cations. The CO axis might be strongly tilted against the surface normal, but as soon as it is rotated horizontally out of the Cr–Cr line, the adsorption energy becomes much smaller.

This behavior is in accord with an electrostatic model of the interaction: The favorable adsorption geometries are those configurations in which the negative parts of the CO quadrupole moment, i.e. the two terminal lone pairs, point towards the surface cations while the positive center of CO is above the O^{2-} anions in the second layer (compare Fig. 2). This picture is in accord with the ARUPS experiments of Xu et al. [1], which showed that the CO molecules are adsorbed flat or strongly tilted on the $Cr_2O_3(0001)$ surface and form a $(\sqrt{3}\times\sqrt{3})R30°$ overlayer. This structure can be most easily explained by assuming that the CO molecules are aligned along the Cr–Cr axes.

Fig. 3 contains the full SCF results for the interaction of a single CO molecule with the embedded $Cr_2O_6^{6-}$ cluster. For each value of the tilt angle θ, two coordinates defining the position of the CO molecule are optimized, namely the center of mass coordinates Z (perpendicular to the $Cr_2O_3(0001)$ plane) and X (along the Cr–Cr line), while Y (perpendicular to the Cr–Cr line) and the azimuthal angle φ are fixed in such a way that CO lies exactly in the plane spanned by the Cr–Cr axis and the surface normal. $\theta = 0°$ and 180° correspond to the atop position of CO on one Cr^{3+} ion (denoted by "Cr-ontop" in the following) with C and O pointing towards the surface, respectively, while $\theta = -90°$ and $+90°$ correspond to CO flat on the surface, either above one O^{2-} anion ("O-ontop" position) or above the hollow spanned by three O^{2-} anions in the second layer (O_3-hollow position).

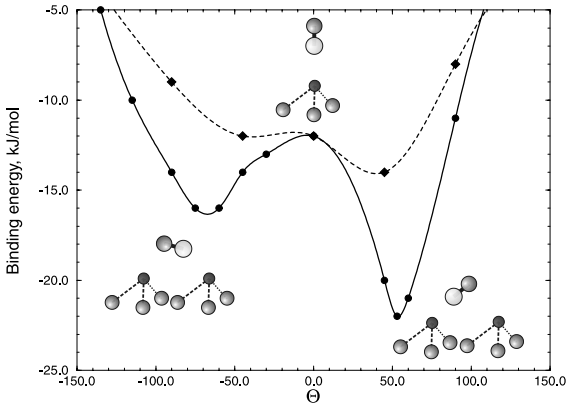

Fig. 3. Potential energy curves for the interaction of CO with the $Cr_2O_3(0001)$ surface. SCF approximation; embedded $Cr_2O_6^{6-}$ cluster. (●) 40% and (◆) 60% relaxation of the topmost Cr–O interlayer distance.

Fig. 3 shows that CO is bound to the Cr_2O_3-(0001) surface by about 13 kJ/mol in the Cr-ontop position with the C atom down. This position is known to be the favorable adsorption geometry for CO on several metal and metal oxide surfaces and has been assumed to be the equilibrium geometry for $CO/Cr_2O_3(0001)$ as well [11]. However, our SCF calculations reveal unambiguously, that the interaction becomes more attractive as soon as CO is allowed to tilt and to move along the Cr–Cr line. Two minima are found: a local minimum with $\theta \approx -75°$, i.e. CO nearly flat on the surface in the O-ontop position, and the absolute minimum with $\theta \sim 55°$ and CO in the O_3-hollow position.

As we have mentioned before, the interaction energy as well as the adsorption geometry depend quite sensitively on the relaxation model used for the cluster. This is evident from Fig. 3 which contains two potential curves, one for 40% and one for 60% relaxation. The two models yield very similar results for $\theta = 0°$, but differ considerably for strongly tilted geometries. The source for this difference is the Pauli repulsion between CO and the O^{2-} anions in the second layer. It is stronger and the interaction is less attractive in the model with the 60% relaxation, i.e. with the small Cr–O interlayer distance, because the CO molecule bound to the two surface Cr ions will come closer to the O^{2-} anions in the second layer. The difference between the adsorption energies of the two minima is caused by the Pauli repulsion as well; the minimum at ~55° is deeper because CO is tilted to a hollow position between three O^{2-} anions where the Pauli repulsion is smaller than in the O-ontop position.

In Fig. 4, we present a 2D plot of the interaction potential ($Y = 0$ and $\varphi = 0$ fixed, Z optimized for each point). It exhibits pronounced valleys

running diagonally through the X, θ plane. This means that a cart-wheel motion of CO on the $Cr_2O_3(0001)$ surface, where a change in the tilt angle θ is accompanied by a lateral translation along the Cr–Cr line, is easily possible since it has to pass only small energy barriers from one O-ontop or O_3-hollow minimum to the adjacent one. In contrast to this, a motion along X without a change in θ and similarly a rotation of CO at a fixed position X are much less likely since they are both connected to high barriers. We think that this topology of the $CO/Cr_2O_3(0001)$ ground state potential is the origin of the stereodynamics observed by Beauport et al. [42] in the laser-induced desorption of CO from $Cr_2O_3(0001)$, but a definite conclusion is only possible after the quantum

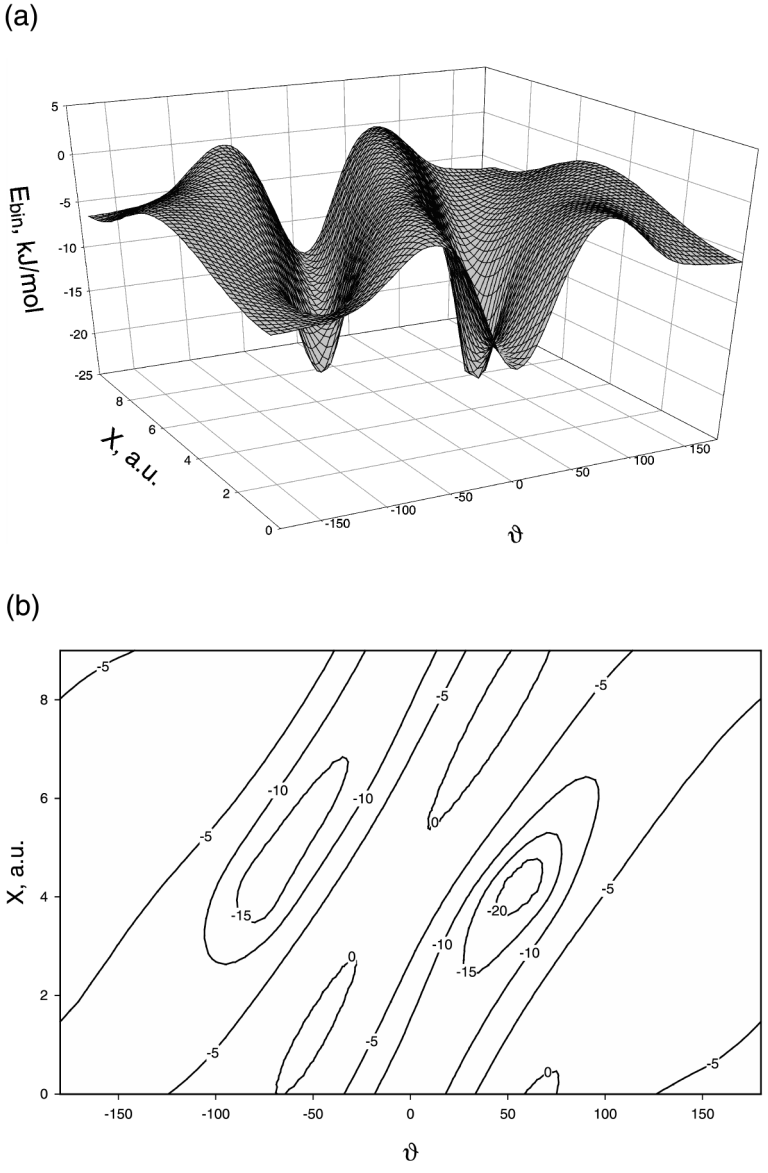

Fig. 4. 2D potential energy surface for $CO/Cr_2O_3(0001)$. SCF approximation, embedded $Cr_2O_6^{6-}$ cluster, 40% relaxation: (a) perspective view, (b) contour plot.

Table 3
Calculated equlibrium geometries and adsorption energies for $CO/Cr_2O_3(0001)$

Position	Cluster	Relaxation (%)	Method	Z^a (a.u.)	X^a (a.u.)	ϑ (°)	E_{ads} (kJ/mol)
Cr-ontop	CrO_3^{3-}	60	SCF	6.6	0.0	0	−13.2
	CrO_3^{3-}	60	MCCEPA[b]	6.6	0.0	0	−13.5
	Cr_4O_6	40	SCF	6.5	0.0	0	−12.8
O-ontop	Cr_4O_6	60	SCF	6.0	6.5	−45	−12.9
	$Cr_2O_6^{6-}$	40	SCF	4.4	4.5	−75	−16.8
	Cr_4O_6	40	SCF	4.4	4.8	−70	−14.4
O_3-hollow	Cr_4O_6	60	SCF	5.3	3.8	45	−14.0
	Cr_4O_6	40	SCF	4.4	4.6	60	−19.7
	$Cr_2O_6^{6-}$	40	SCF	4.4	4.3	53	−22.3
	$Cr_2O_6^{6-}$	40	MCCEPA[c]	4.4[d]	4.3[d]	53[d]	−27.8
	$Cr_2O_6^{6-}$	40	SCF	3.9[d]	4.3[d]	53[d]	−17.2
	$Cr_2O_6^{6-}$	40	MCCEPA[c]	3.9[d]	4.3[d]	53[d]	−27.6

[a] Center of mass coordinates of CO; Z relative to the first Cr layer.
[b] Extended basis set; valence electrons of CO and 3d electrons of the Cr^{3+} ion are included in the correlation treatment.
[c] Extended basis set; valence electrons of CO, 3d electrons of both Cr^{3+} ions and valence electrons (localized orbitals) of the closest O^{2-} anions in the second layer are included in the correlation treatment.
[d] Fixed geometry; single-point calculation.

mechanical simulation of the desorption dynamics has been performed [43].

Table 3 contains the details of the calculated equilibrium geometries and adsorption energies for the Cr-ontop position and the two tilted configurations. In addition to the SCF results we have included the results of a few single-point MCCEPA calculations. In these calculations all valence electrons of CO and the surface Cr ions were included in the correlation space as well as the valence electrons of the closest O^{2-} anions in the $Cr_2O_6^{6-}$ cluster. The basis sets both at CO and the cluster had to be extended considerably to account for an appreciable part of the intermolecular correlation energy. The results in Table 3 show that electron correlation does not much change the adsorption energy for the Cr-ontop position. For the strongly tilted O_3-hollow minimum, on the other hand, electron correlation leads to a larger adsorption energy as well as to a shorter distance between CO and the surface.

One should not take the results of Table 3 too literally. First of all, the calculated adsorption energies depend to some extent on the relaxation of the topmost interlayer distance, which is not known precisely, and also on the embedding and on the size of the cluster. Furthermore, only part of the intermolecular correlation is covered by the MCCEPA calculations since only a few of the electrons of the Cr_2O_3 substrate are included in the correlation treatment. The high numerical expense (many electrons to correlate, large basis sets necessary) is prohibitive for extending the MCCEPA calculations to correlate more than just a few surface atoms.

To conclude, our calculations predict a $CO/Cr_2O_3(0001)$ equilibrium structure with a strongly tilted CO in the O_3-hollow position and an adsorption energy of about 22 kJ/mol (SCF) and 28 kJ/mol (MCCEPA). This value might be enhanced by ~5 kJ/mol if the full CO/Cr_2O_3 van der Waals attraction is accounted for. The binding energies for CO in the Cr-ontop position and in the O-ontop position (tilt angle $\theta = -70°$) are much smaller, only in the order of 13–15 kJ/mol, however, the Cr-ontop position is not a local minimum, i.e. no stable adsorption geometry. We therefore expect that the preferred adsorption at low CO coverage will take place exclusively in the O_3-hollow equilibrium structure.

2.5. CO stretching frequency

Frequencies for the CO stretching vibration were calculated for the three adsorption positions described above, both at the SCF and MCCEPA

levels. A slightly extended basis was used, in which the standard basis set of Table 2 was augmented by one f set at C and O (TZ2DF basis). In the MCCEPA calculations, only the orbitals at CO and the 3d electrons at the Cr^{3+} ions were correlated.

Generally, SCF results for vibration frequencies have large errors, which amount to about 260 cm^{-1} in the case of CO, and even the MCCEPA results with the TZ2DF basis are not accurate enough to allow for unique assignments. We have therefore treated the isolated CO molecule in the same way as the adsorbed one since the calculated frequency shifts are more reliable than the frequencies themselves. In all cases, we have directly calculated the observable fundamental frequency, i.e. the $\Delta G_{1/2}$ value, and not the harmonic frequency. The experimental value for the isolated CO molecule is 2143 cm^{-1} [44].

Our results in Table 4 show that the stretching frequency of CO adsorbed in the Cr-ontop position experiences a blue shift of about 15 cm^{-1}. SCF and MCCEPA do not differ much. Such a shift is typical for CO adsorbed normal to the surface at the cations of metal oxides and has been attributed to the ''wall effect'' by Pacchioni et al. [45].

The frequency shifts for the two tilted adsorption positions are somewhat unexpected. In the SCF approximation red shifts are found for both adsorption geometries, but correlation effects yield additional blue shifts of about 20–30 cm^{-1}. At the O-ontop position, the overall shift is rather small and negative, at the O_3-hollow position an appreciable blue shift results. All shifts become larger when the CO molecule is approaching closer to the surface. For the most probable distance between CO and the surface ($Z = 3.9$ a.u. for both positions, i.e. 0.5 a.u. closer than the SCF minimum) shifts of -5 and $+22$ cm^{-1} for the two adsorption positions are obtained.

The small red shifts obtained at the SCF level can be rationalized by a certain amount of covalent bonding between CO and the two surface Cr ions, i.e. a $3d \rightarrow \pi^*$ backdonation which weakens the C–O bond and lowers the C–O stretching frequency. This effect is more pronounced for CO molecules adsorbed parallel to the surface than for those normal to the surface. Furthermore, the electrostatic potential above the surface has also some effect on the CO frequency. Therefore, modifications in the embedding PC field lead to small changes in the vibration frequencies, but the main trend is unaltered.

3. Experiments

3.1. Experimental setup

The TDS and IRAS experiments have been performed in an ultrahigh vacuum system with a base pressure of 3×10^{-10} mbar. A detailed de-

Table 4
Calculated CO stretching frequencies (in cm^{-1})[a,b,c]

Position	Z (a.u.)	Cluster	Method	CO isolated	CO adsorbed	Frequency shift
Cr-ontop ($\theta = 0°$)	6.6	CrO_3^{3-}	SCF	2401	2415	+14
			MCCEPA	2203	2220	+17
O-ontop ($\theta = -75°$)	4.4	$Cr_2O_6^{6-}$	SCF	2400	2378	−22
			MCCEPA	2201	2200	−1
	3.9	$Cr_2O_6^{6-}$	SCF	2399	2363	−36
			MCCEPA	2202	2197	−5
O_3-hollow ($\theta = 53°$)	4.4	$Cr_2O_6^{6-}$	SCF	2400	2392	−8
			MCCEPA	2202	2210	+8
	3.9	$Cr_2O_6^{6-}$	SCF	2400	2397	−3
			MCCEPA	2202	2224	+22

[a] Fundamental frequencies, $\Delta G_{1/2}$.
[b] Standard basis, see Table 2, augmented by one f set on C and O with the exponents 0.8 and 1.4, respectively.
[c] There are slight variations in the results for the isolated CO molecule, since the calculations were performed in exactly the same way (orientation of the CO axis, localization of the orbitals etc.) as for the adsorbed CO molecules.

scription of the experimental setup is given in Refs. [46,47]. Briefly, the apparatus is equipped with an Omicron 4 grid-spectraleed optics for LEED and Auger spectroscopy and a VSW quadrupole mass spectrometer and a specially designed doser system for TDS. A modified Mattson RS-1 FTIR spectrometer is attached to KBr-windows of the UHV chamber to perform IRAS measurements in grazing incidence geometry.

The chromium oxide film with (0001) orientation was prepared via oxidation of a Cr(110) single crystal according to well-known recipes [1,2,18,48–50]. The film thickness is about 40 Å. Concerning the IRAS measurements, the reflectivity of the sample is still very high due to the metal support. Also the surface selection rule of IRA-spectroscopy on metal substrates [51] still holds for thin films grown on metal single crystals, so-called buried metal layer (''BML'') systems [52].

The IR single beam spectra were recorded with a spectral resolution of 2 cm^{-1} accumulating 500 scans. The transmittance spectra were calculated from the single beam spectra of the clean and the adsorbate-covered surface. Afterwards they were baseline corrected.

3.2. Results

Fig. 5 shows CO TD-spectra from the Cr_2O_3-(0001) surface as a function of initial dosage at 90 K. At low exposures (0.2 L) we observe a desorption feature at about 180 K. While the dosage is increased the signal gains intensity and slightly shifts to 175 K. The intensity reaches saturation for an exposure of 2.5 L. As the signal maximum is almost independent of the CO coverage we identify first order desorption which is typical for undissociated adsorbed molecules. On the basis of the Redhead formula [53] the activation energy for the desorption is estimated to be about 45 kJ/mol. Therefore, the appropriate state may be termed chemisorbed.

If the CO exposure exceeds 2.5 L a second desorption feature can be observed at 105 K. This peak can be associated with more weakly bound CO molecules which are adsorbed in addition to the chemisorbed CO. The saturation of the surface is achieved by a dosage of about 5 L. Multilayer

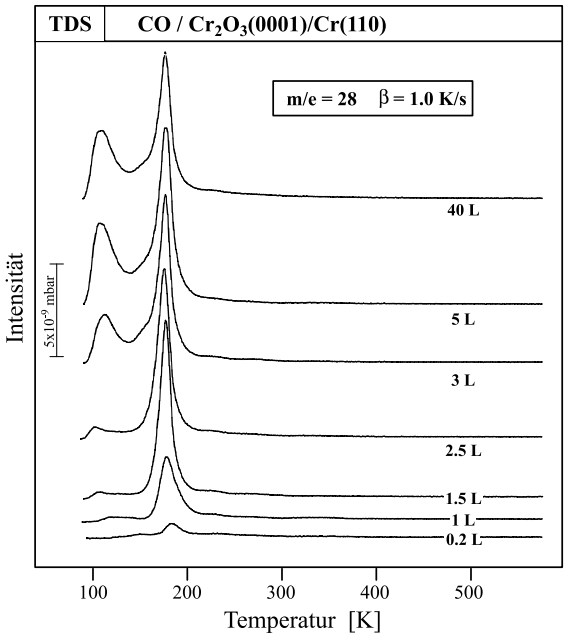

Fig. 5. Thermal desorption spectra ($m/e = 28$) of CO from Cr_2O_3(0001)/Cr(110) for various dosages.

adsorption of CO does not occur on Cr_2O_3(0001)/Cr(110) at 90 K.

The IR-spectra confirm the presence of different CO species on Cr_2O_3(0001). Fig. 6 shows a series of IRAS-spectra as a function of initial CO dosage at 90 K. Using a CO-exposure of 0.05 L we detect a signal of the CO-stretching vibration at 2178 cm^{-1} and at 0.1 L a second signal appears at 2165 cm^{-1}. With increasing coverage the high-frequency signal considerably increases and slightly shifts to lower wave numbers. The weak signal at 2165 cm^{-1} does not gain further intensity. Instead it disappears in the shoulder of the main signal. Finally, at exposures above 3 L a third signal appears at 2136 cm^{-1}. For saturation coverage (5 L CO, topmost spectrum) we measure absorption maxima at 2170 and 2132 cm^{-1}, respectively.

If the coverage dependence of the IRAS and TDS spectra (Figs. 5 and 6) is compared the different signals can be correlated. The IR-feature at 2170 cm^{-1} as well as the desorption maximum at 175 K are assigned to the chemisorbed CO-species. Its adsorption site is occupied at low CO exposure. The more weakly bound state is observed at

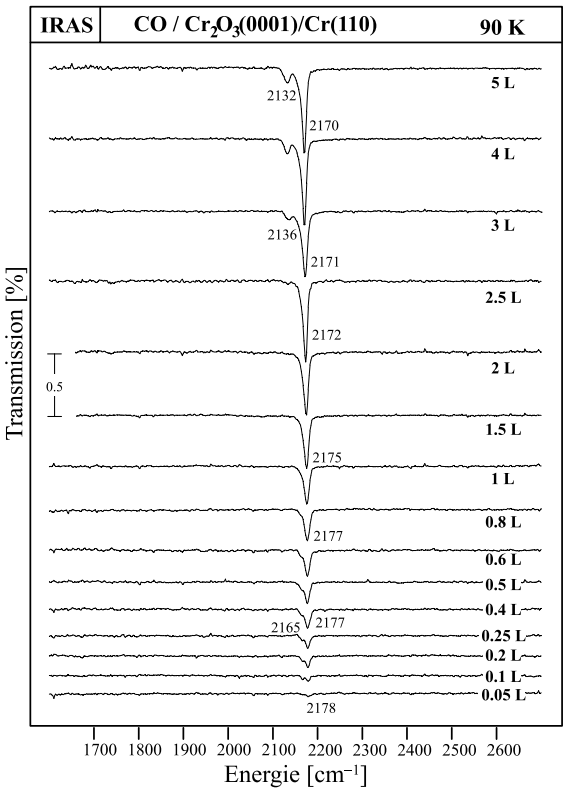

Fig. 6. Infrared reflection adsorption spectra of CO adsorbed on $Cr_2O_3(0001)/Cr(110)$ as a function of dosage at 90 K.

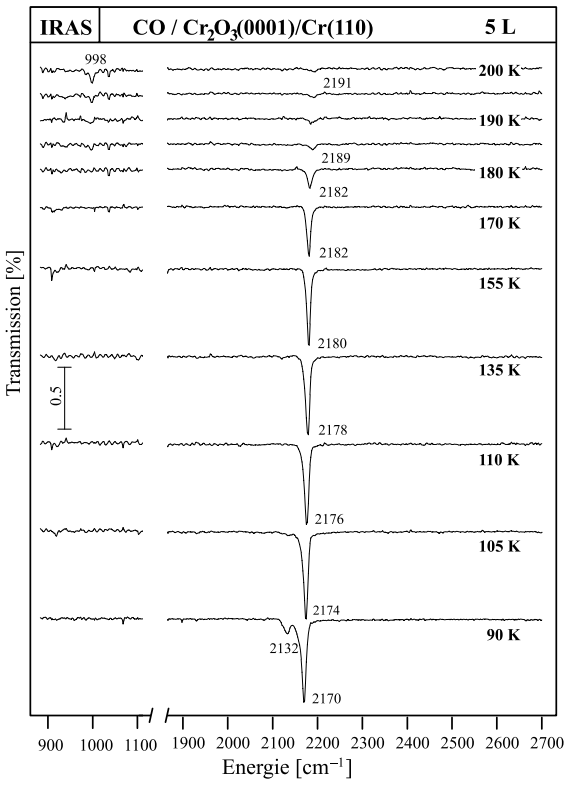

Fig. 7. Infrared reflection adsorption spectra of CO adsorbed on $Cr_2O_3(0001)/Cr(110)$ as a function of temperature after dosing 5 L at 90 K.

CO exposures exceeding 3 L. This adsorbate species is characterized by the stretching vibration at 2132 cm^{-1} and the desorption signal at 105 K.

Heating experiments support the assignment of the IR features to the TDS maxima. Fig. 7 shows IRA-spectra which are measured after annealing the adsorbate covered substrate to temperatures up to 200 K. (For technical reasons the data acquisition itself has to be performed each time after recooling to 90 K.) In fact, after slight annealing to 105 K the IR feature at 2132 cm^{-1} diminishes whereas the intensity of the main signal shows no significant changes in the temperature regime between 90 and 155 K. However the signal slightly shifts to higher wave numbers ($\approx$2180 cm^{-1}). Upon further heating, we observe the attenuation of the main IR-signal which runs parallel to the desorption at about 175 K in the TDS.

A blue shift of the stretching vibration has been frequently observed for CO adsorbed on transition metal oxides. While only few vibrational studies have been reported for single crystal oxide surfaces (e.g. CO on CoO [54,55] and NiO [55–57]) many IR experiments have been performed on polycrystalline materials (overviews in [3,10]). CO adsorption on powder samples of α-chromium oxide has been studied by several authors (Zaki and Knözinger [4], Hadjiivanov and Busca [5] and Zecchina and coworkers [6–10]). At high CO coverages the dominant feature of the IR spectra was congruently detected at 2167 cm^{-1} and assigned to CO adsorbates standing on the surface chromium ions. Zecchina and coworkers [10] also investigated the coverage dependence of CO adsorption on microcrystalline Cr_2O_3 samples. At 77 K the main IR signal is shifted from 2181 cm^{-1} at low CO exposures to 2167 cm^{-1} at saturation

coverage. This result is comparable to the coverage dependence of the high frequency IR signal of the CO/Cr_2O_3(0 0 0 1) system shown in Fig. 6, although the microcrystals are thought to expose mainly unpolar (0 1 $\bar{1}$ 2) facets terminated by chromium ions in fivefold square pyramidal coordination.

4. Discussion

Cluster calculations and TDS measurements yield a consistent picture of the adsorption of CO on the Cr_2O_3(0 0 0 1) surface in the low coverage regime. The pronounced desorption peak observed at 175 K in attributed by means of the cluster calculations to the adsorption of an undissociated CO molecule, bound in the most stable adsorption position. This is the O_3-hollow position, with the CO axis strongly tilted against the surface normal and oriented along a line connecting two Cr ions at the surface. This picture is also consistent with previous ARUPS and NEXAFS experiments [1,2], which revealed that CO is adsorbed strongly tilted or nearly flat on the Cr_2O_3(0 0 0 1) surface. However, the ARUPS and NEXAFS measurements had to be performed at a rather high background CO pressure of 1×10^{-8} mbar, therefore they correspond to the high coverage limit and cannot be directly compared with the present calculations.

Unfortunately, considerable discrepancy exists concerning the adsorption energy. The value of 45 kJ/mol estimated from the TDS peak by means of the Redhead formula [53] is much larger than our calculated MCCEPA value of 28 kJ/mol. Even if we allow for about 5 kJ/mol for adsorbate-induced relaxations (Section 2.2.) and 5 kJ/mol for the extracluster van der Waals attraction (Section 2.4.), our estimate of 38 kJ/mol is still too low. The remaining error is mainly caused by the uncertainty of the topmost interlayer spacing. However, one should keep in mind that similar and even larger deviations between TDS and ab initio adsorption energies were found for related systems, for instance for CO and NO on NiO(1 0 0) [58,59]. It seems that neither the cluster approach nor the periodic supercell approach can give a quantitatively satisfactory theoretical answer for adsorption energies.

In any case, it is justified to call the adsorption of CO in the O_3-hollow position a "chemisorption". The dominant contribution to the interaction energy has electrostatic origin and is caused by the attraction of the quadrupole moment of CO in the strongly inhomogeneous electrostatic field above the Cr_2O_3(0 0 0 1) surface.

Reasonable agreement between theory and experiment exists also for the frequency shift of the CO stretching vibration. Our calculations predict a blue shift of $+22$ cm^{-1} for CO in the O_3-hollow position, see Table 4. This compares favorably with the experimental shift of $+35$ cm^{-1} observed for the most prominent IRAS peak in the low coverage limit. There is no doubt that inclusion of extracluster van der Waals effects in the calculation would move the CO molecule in the O_3-hollow position closer to the surface and would lead to a slightly larger blue shift and to a better agreement with the experimental IRAS peak.

It is much more difficult to assign the second TDS peak at 105 K which appears at higher CO coverages and is accompanied by a second IRAS band at 2132 cm^{-1}, i.e. a band with a small red shift of about -10 cm^{-1}. One might be tempted to attribute this feature to CO molecules adsorbed in the O-ontop position, i.e. in the local minimum with CO nearly parallel to the surface. Such an assignment is supported by the calculated adsorption energy of 15 kJ/mol, which exhibits a similar deviation from the TDS value of 28 kJ/mol as does the adsorption energy for the O_3-hollow position. Furthermore, we calculate a small red shift of -5 cm^{-1} for the CO stretching vibration in this position which fits quite well to the experimental shift of about -10 cm^{-1}. And finally, the LEED, ARUPS and NEXAFS measurements of Xu and coworkers [1,2] showed that at higher coverages a stable or at least metastable CO overlayer on Cr_2O_3(0 0 0 1) exists with strongly tilted CO molecules (tilt angle 70–80°). Thus, TDS and IRAS experiments can be interpreted in such a way that first, at low coverages, the O_3-hollow positions will be occupied by CO molecules, and then at higher coverages, when the O_3-hollow positions are fully occupied, CO will be adsorbed in the O-ontop positions. (It should be mentioned that the desorption temperature of 105 K is much

larger than the typical desorption temperature of 30–40 K for the CO multilayer adsorption [59], therefore the TDS peak at 105 K must reflect some $CO/Cr_2O_3(0001)$ interaction and is not a pure multilayer desorption peak.)

However, the present calculations were performed for a single CO molecule adsorbed on $Cr_2O_3(0001)$ and no lateral CO–CO interactions were accounted for. Therefore, the discussion of the high-coverage state remains to some extent speculative. It could be possible as well that the weakly bound O-ontop position is blocked or strongly modified by CO molecules adsorbed in O_3-hollow positions nearby or that a new adsorption position in the second layer is formed by a combination of $CO/Cr_2O_3(0001)$ attraction and lateral CO–CO interaction. In order to address this question we are currently performing Monte Carlo simulations [12] for the high coverage regime using the potential energy surface calculated in the present study and a gas phase CO–CO interaction potential from the literature [60].

Acknowledgements

This study was financially supported by Deutsche Forschungsgemeinschaft, Ministerium für Wissenschaft und Forschung des Landes Nordrhein-Westfalen, Fonds der Chemischen Industrie, and by the Max-Planck society. M.P. benefited from a grant of the graduate college "Dynamische Prozesse an Festkörperoberflächen". The authors thank Dr. H. Kuhlenbeck, Fritz-Haber-Institut, Berlin, for his assistance with the experiments and many stimulating discussions.

References

[1] C. Xu, B. Dillmann, H. Kuhlenbeck, H.-J. Freund, Phys. Rev. Lett. 67 (1991) 3551.
[2] H. Kuhlenbeck, C. Xu, B. Dillmann, M. Haßel, B. Adam, D. Ehrlich, S. Wohlrab, H.-J. Freund, U.A. Ditzinger, H. Neddermeyer, M. Neuber, M. Neumann, Ber. Bunsenges. Phys. Chem. 96 (1992) 15.
[3] A.A. Davydov, Infrared Spectroscopy of Adsorbed Species on the Surface of Transition Metal Oxides, Wiley, Chichester, New York, 1990.
[4] M.I. Zaki, H. Knözinger, J. Catal. 119 (1989) 311.
[5] K. Hadjiivanov, G. Busca, Langmuir 10 (1994) 4534.
[6] D. Scarano, A. Zecchina, Spectrochim. Acta 43A (1987) 1441.
[7] D. Scarano, A. Zecchina, A. Reller, Surf. Sci. 198 (1988) 11.
[8] D. Scarano, A. Zecchina, S. Bordiga, G. Ricchiardi, G. Spoto, Chem. Phys. 177 (1993) 547.
[9] D. Scarano, G. Spoto, S. Bordiga, G. Ricchiardi, A. Zecchina, J. Electron Spectrosc. Relat. Phenom. 64/65 (1993) 307.
[10] A. Zecchina, D. Scarano, S. Bordiga, G. Ricchiardi, G. Spoto, F. Geobaldo, Catal. Today 27 (1996) 403.
[11] D. Scarano, G. Ricchiardi, S. Bordiga, P. Galletto, C. Lamberti, G. Spoto, A. Zecchina, Faraday Disc. 105 (1996) 119.
[12] M. Pykavy, V. Staemmler, in press.
[13] R.W.G. Wyckoff, Crystal structures, Second ed., Vol. II, Wiley, New York, 1964, p. 6.
[14] P.W. Tasker, J. Phys. C: Solid State Phys. 12 (1979) 4977.
[15] P.W. Tasker, Phil. Mag. A 39 (1979) 119.
[16] H.-J. Freund, H. Kuhlenbeck, V. Staemmler, Rep. Prog. Phys. 59 (1996) 283.
[17] J.A. Mejias, V. Staemmler, H.-J. Freund, J. Phys.: Condens. Matter 11 (1999) 7881.
[18] F. Rohr, M. Bäumer, H.-J. Freund, J.A. Mejias, V. Staemmler, S. Müller, L. Hammer, K. Heinz, Surf. Sci. 372 (1997) L291.
[19] A.J. Rowley, M. Wilson, P.A. Madden, J. Phys.: Condens Matter 11 (1999) 1903.
[20] C. Rehbein, N.M. Harrison, A. Wander, Phys. Rev. B 54 (1996) 14066.
[21] A. Leitheußer, Ph.D. Thesis, Ruhr-Universität Bochum, 2000.
[22] K. Wolter, D. Scarano, J. Fritsch, H. Kuhlenbeck, A. Zecchina, H.-J. Freund, Chem. Phys. Lett. 320 (2000) 206.
[23] F. Rohr, M. Bäumer, H.-J. Freund, J.A. Mejias, V. Staemmler, S. Müller, L. Hammer, K. Heinz, Surf. Sci. 389 (1997) 391.
[24] Th. Gloege, H.L. Meyerheim, W. Moritz, D. Wolf, Surf. Sci. 441 (1999) L917.
[25] F. Rittner, R. Fink, B. Boddenberg, V. Staemmler, Phys. Rev. B 57 (1998) 4160.
[26] H.M. Evjen, Phys. Rev. 39 (1932) 675.
[27] L.Z. Stolarczyk, L. Piela, Int. J. Quantum Chem. 22 (1982) 911.
[28] L. Piela, J.L. Brédas, J.M. André, J. Chem. Phys. 78 (1983) 295.
[29] M. Wierzbowska, J. Wasilewski, V. Staemmler, in press.
[30] A. Bergner, M. Dolg, W. Kuechle, H. Stoll, H. Preuss, Mol. Phys. 80 (1993) 1431.
[31] V. Staemmler, Theor. Chim. Acta 45 (1977) 89.
[32] J. Wasilewski, Int. J. Quantum Chem. 36 (1989) 503.
[33] U. Meier, V. Staemmler, Theor. Chim. Acta 76 (1989) 95.
[34] R. Fink, V. Staemmler, Theor. Chim. Acta 87 (1993) 129.
[35] E.J. Samuelsen, M.I. Hutchings, G. Shirane, Physica 48 (1970) 13.

[36] A.J.H. Wachters, J. Chem. Phys. 52 (1970) 1033.
[37] M. Dolg, U. Wedig, H. Stoll, H. Preuss, J. Chem. Phys. 86 (1987) 866.
[38] S. Huzinaga, Approximate atomic functions, I. Technical report, University of Alberta, Canada, 1971.
[39] W.L. Meerts, F.H. De Leeuw, A. Dymanus, Chem. Phys. 22 (1977) 319.
[40] S.F. Boys, F. Bernardi, Mol. Phys. 19 (1970) 553.
[41] S.S. Xantheas, J. Chem. Phys. 104 (1996) 8821.
[42] I. Beauport, K. Al-Shamery, H.-J. Freund, Chem. Phys. Lett. 256 (1996) 641.
[43] S. Thiel, T. Klüner, H.-J. Freund, M. Pykavy, V. Staemmler, in press.
[44] K.P. Huber, G. Herzberg, Constants of diatomic molecules, Van Nostrand Reinhold, New York, 1979.
[45] G. Pacchioni, C. Gogliandro, P.S. Bagus, Int. J. Quantum Chem. 42 (1992) 1115.
[46] O. Seiferth, Ph.D. Thesis, Ruhr-Universität Bochum, 1997.
[47] B. Dillmann, Ph.D. Thesis, Ruhr-Universität Bochum, 1996.
[48] C.A. Ventrice Jr., D. Ehrlich, E.L. Garfunkel, B. Dillmann, D. Heskett, H.-J. Freund, Phys. Rev. B46 (1992) 12892.
[49] M. Bender, D. Ehrlich, I.N. Yakovkin, F. Rohr, M. Bäumer, H. Kuhlenbeck, H.-J. Freund, V. Staemmler, J. Phys.: Condens. Matter 7 (1995) 5289.
[50] C. Xu, M. Haßel, H. Kuhlenbeck, H.-J. Freund, Surf. Sci. 258 (1991) 23.
[51] B.E. Hayden, Vibrational spectroscopy of molecules on surfaces, in: J.T. Yates, T.E. Madey (Eds.), Methods of Surface Characterization, Vol. 1, Plenum, New York, 1987 (Chapter 7).
[52] V.M. Bermudez, J. Vac. Sci. Technol. A10 (1992) 152.
[53] P.A. Redhead, Vacuum 12 (1962) 203.
[54] M. Haßel, Ph.D. Thesis, Ruhr-Universität Bochum, 1995.
[55] M. Schönnenbeck, D. Cappus, J. Klinkmann, H.-J. Freund, L.G.M. Pettersson, P.S. Bagus, Surf. Sci. 347 (1996) 337.
[56] D. Cappus, Ph.D. Thesis, Ruhr-Universität Bochum, 1995.
[57] S.M. Vesecky, C. Xu, D.W. Goodman, J. Vac. Sci. Technol. A12 (1994) 2114.
[58] H.-J. Freund, Faraday Discuss. Chem. Soc. 114 (1999) 1.
[59] R. Wichtendahl, M. Rodriguez-Rodrigo, U. Härtel, H. Kuhlenbeck, H.-J. Freund, Surf. Sci. 423 (1999) 90.
[60] W.B.J.M. Janssen, J. Michiels, A. van der Avoird, J. Chem. Phys. 94 (1991) 8402.